Polymer Vol. 37 No. 11, pp. 2259–2272, 1996

0032-3861/96/$15.00 + 0.00

Phase-separated structures formed in polymer mixtures containing a thermotropic liquid crystalline copolyester as one component

Akemi Nakai*, Toshio Shiwaku†, Wei Wang, Hirokazu Hasegawa and Takeji Hashimoto‡
Division of Polymer Chemistry, Graduate School of Engineering, Kyoto University, Kyoto 606-01, Japan
(Received 24 July 1995; revised 21 September 1995)

The phase-separated structures formed in polymer mixtures consisting of a thermotropic liquid crystalline copolyester and poly(ethylene terephthalate) (PET) are investigated. The 50 wt%/50 wt% mixtures isotropic, transparent and homogeneous were prepared by dissolution of the copolyester and PET in an organic solvent followed by rapid removal of the solvent. Their phase separation processes during isothermal annealing at various temperatures after rapidly heating the as-prepared thin films were investigated by real-time and *in situ* polarized light microscopy and light scattering. At the annealing temperature below the melting point of PET ($T_{m,PET}$), the vitrification and crystallization of the components strongly affect phase separation, giving rise to pinning of the coarsening process at the different stages of phase separation and hence leading to various phase-separated structures. Rapid phase separation via spinodal decomposition was observed at annealing temperatures above $T_{m,PET}$. The phase-separated structures were found to evolve via the following sequence of mechanisms: (1) self-similar growth of the percolated networks of the anisotropic and isotropic phases; (2) disruption of the percolated network and formation of anisotropic droplets in the isotropic matrix; and (3) coalescence of anisotropic droplets. Light scattering from the percolated network structure was further investigated in terms of the spatial distributions of the orientation and concentration fluctuations. Copyright © 1996 Elsevier Science Ltd.

(Keywords: thermotropic LC copolyester; poly(ethylene terephthalate); polymer mixture)

INTRODUCTION

Ever since some commercial main-chain thermotropic liquid crystalline (LC) copolymers were successfully prepared[1–3], some of their novel and excellent properties have attracted the attention of scientists and engineers, promoting widespread and profound investigations on the rheological properties[4–8], the supermolecular structures and optical textures[9–21], as a function of temperature or annealing time, and the phase transitions[22–29] in the crystalline, liquid crystalline and isotropic liquid states. Nowadays, much more emphasis in the applications of the LC copolyesters is placed on blending or alloying them with conventional engineering plastics to improve their 'processability' and mechanical properties, as reviewed elsewhere[30]. An important concept used in the preparation of such blends or alloys is that of the 'molecular composite', meaning that the semiflexible LC macromolecules are molecularly dispersed in conventional plastics and hence the reinforcement takes effect at the molecular level[31–35]. This concept has promoted investigations of the phase separation processes and the phase-separated structures of blends of LC polymers with conventional plastics[36–40]. Some theoretical studies on the miscibility of such blends show that it is necessary to take two order parameters, concentration fluctuation and orientation fluctuation, into account in order to describe their phase behaviour[41–45]. The latter parameter demonstrates the influence of the liquid crystalline nature of one component on the miscibility of the blends. In this study we call this effect the 'LC effect'.

In this paper, as an extension of our previous study[36,37], we present our experimental results on phase-separated structures formed by phase separation via spinodal decomposition (SD) in polymer mixtures with a thermotropic liquid crystalline copolyester as one component. During phase separation at temperatures higher than the melting points of the component polymers, the mixture separates into a liquid crystalline phase and an isotropic melt phase. In this case the phase-separated structure can be easily detected by polarized light microscopy and by depolarized or polarized light scattering. The unmixing process and the coarsening

* Present address: Department of Home Economics, Kyushu Women's Junior College, 1-1 Jiyugaoka, Yawatanishi, Kitakyushu 807, Japan
† Present address: Polyplastics Co. Ltd, Research Centre, 973 Miyajima, Fuji City Shizuoka-Pref. 416, Japan
‡ To whom correspondence should be addressed

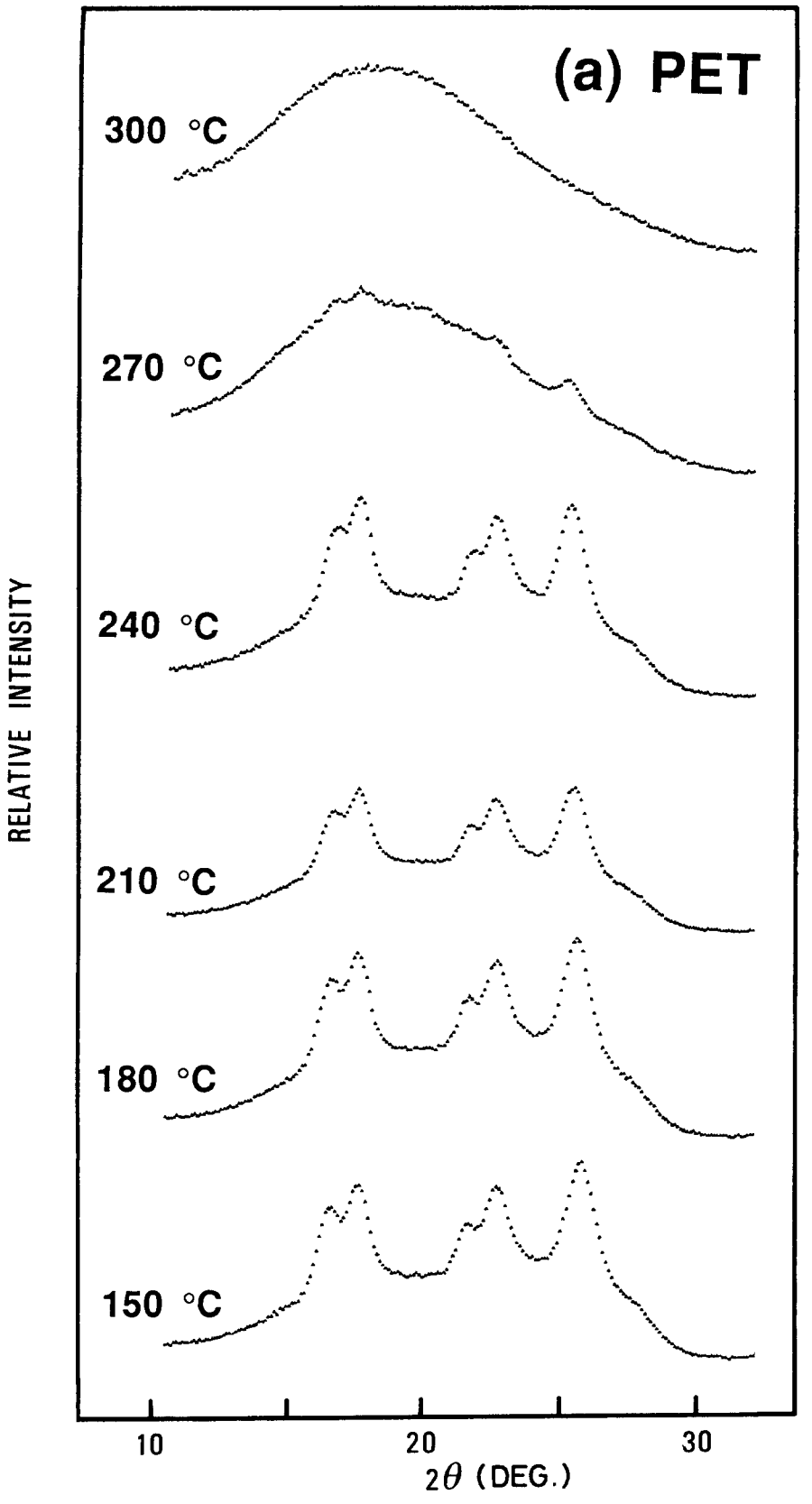

Figure 1 WAXD profiles of neat PET (a) and neat X-7G (b) obtained at 150, 180, 210, 240, 270 and 300°C

process in the mixture via SD will be discussed in detail elsewhere[46]. Because one of the components is a thermotropic LC copolyester, its liquid crystallinity may affect the phase separation and the coarsening process and hence the phase-separated structure to a certain extent. The ordering process that occurs in pure LC liquids[18,19] will also appear in the LC domains after phase separation. Therefore, this phase-separated structure is expected to be different from other optically isotropic blend systems, which we will discuss in this paper.

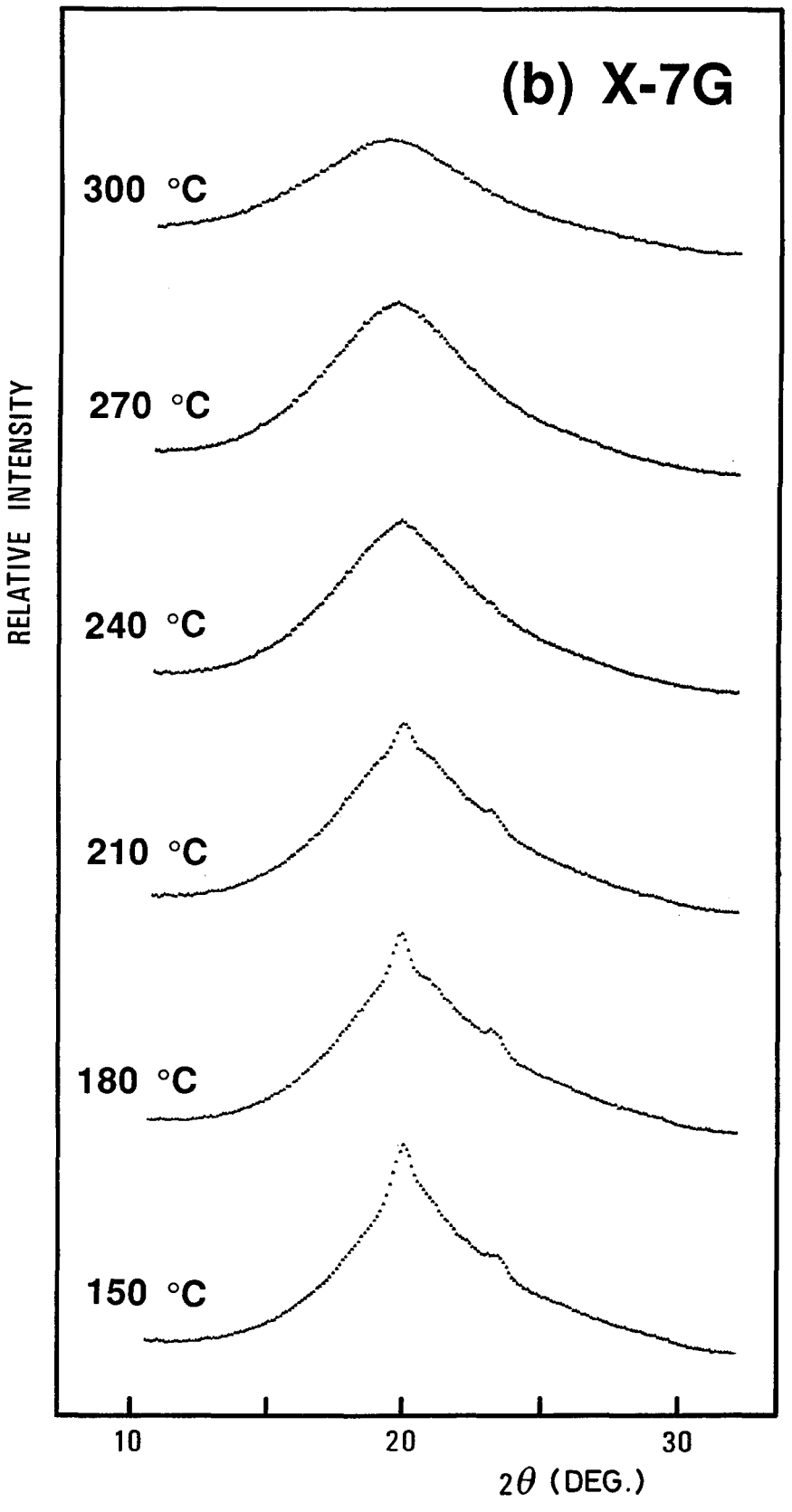

Figure 1. (*Continued*)

EXPERIMENTAL

The materials used in this study were a statistical copolyester containing 60 mol% *p*-oxybenzoate (OBA) and 40 mol% ethylene terephthalate (trade name X-7G, Tennessee Eastman Co. Ltd) and a commercial poly(ethylene terephthalate) (PET) (Toray Co. Ltd). The number-average molecular weights of these polymers were both about 2×10^4. X-7G is a commercial thermotropic main-chain liquid crystalline copolyester,

and its LC properties and supermolecular structure were first investigated by Jackson and Kuhfuss[1]. X-7G was selected as the LC component as it can be dissolved in some organic solvents[18,19,36–39], and homogeneous mixtures with the commercial poly(ethylene terephthalate) (PET) are available.

A mixture of X-7G and PET in a ratio of 50/50 by weight was dissolved in *o*-chlorophenol (about 2 wt% polymers) at 60°C. A small amount of insoluble particles, probably crystallites of pure poly(*p*-oxybenzoate) or copolymers having a much higher OBA content than the average, were carefully removed by filtration. The solution was filtered first through filter paper and subsequently through a Millipore membrane with a pore size of 0.5 μm. One or two drops of the clear solution were cast onto a microscope cover glass, which was then quickly moved into a vacuum oven to evaporate the solvent as quickly as possible at 60°C. Solvent evaporation seemed to be complete within a few minutes, but the film specimens were kept under vacuum for an additional 3 h to remove any remaining solvent.

The films thus prepared had an average diameter of about 10 mm and an average thickness of about 10 μm at the centre, but were somewhat thicker around the edge. Film specimens with a free surface appeared transparent, optically isotropic and homogeneous under optical microscopic observation with or without crossed polarizers, indicating that the polymers in the as-cast films were both in the amorphous glassy state and the two kinds of molecules were uniformly dispersed at a length scale larger than the micrometre level. One of the advantages of using such a quick casting method is that a homogeneous mixture of two immiscible polymers can be obtained. Another advantage is that some complicated chemical reactions in the preparation process of the specimens, such as transesterification and degradation of the polymers during mechanical mixing at an elevated temperature[30], which often lead to a complicated result that is difficult to analyse, can be avoided.

The temperature jump (T-jump) and annealing experiments were performed by placing the film specimens on the cover glass onto a microscope heating stage (TH-600 type, LINKAM Scientific Co.) controlled at various annealing temperatures. The test specimens reached the preset temperatures within a few seconds. The phase separation of the mixtures and subsequent ordering process occurring in the LC domains were investigated by real-time and *in situ* observations under a polarized light microscope (PLM) (Nikon Optiphot-Pol XTP-11) with a roll-film camera and by laser light scattering (LS). For some observations, a red plate with 530 nm retardation was inserted between the crossed polarizers. The advantage of using the red plate has been indicated in a previous paper[47]. Some specimens were quenched from the annealing temperatures to room temperature in order to freeze in the phase-separated structure, and then further investigated by means of the PLM and LS.

In order to isolate the phase-separated structure from the influence of the optically anisotropic nature of the LC domains, we used an optical diffraction method. The PLM micrographs of the phase-separated mixture were first binarized by the method reported elsewhere[46], and then transformed into positive slide films. The binarization eliminated the liquid crystalline textures from the images of the phase-separated structures. The optical diffraction patterns of the slide films were obtained with a helium–neon laser.

Wide angle X-ray diffraction (WAXD) profiles of the specimens of pure X-7G and pure PET were measured *in situ* as a function of temperature. The apparatus consisted of a 12 kW rotating anode X-ray generator (Rigaku Ru-a operating at 50 kV and 200 mA), a graphite monochromator and a one-dimensional position sensitive detector. More details of the apparatus can be found elsewhere[48,49]. CuK_α radiation with a wavelength of 1.54 Å (1 Å = 0.1 nm) was used.

Differential scanning calorimetry (d.s.c.) using a Perkin–Elmer DSC-7 was performed for temperatures between 25 and 300°C at a heating rate of 10°C min^{-1} to measure the thermal transitions in the as-received X-7G and PET pellets.

RESULTS AND DISCUSSION

WAXD and d.s.c.

Prior to WAXD measurements, the as-received pellets of X-7G and PET were dried under vacuum at 60°C for 24 h to avoid hydrolysis at high temperatures. The crystalline PET specimen was prepared by annealing the PET pellets in an X-ray sample holder under an N_2 atmosphere at 180°C (a typical crystallization temperature) for 10 h. The X-7G pellets were annealed at 260°C for 10 h in the sample holder under an N_2 atmosphere and then slowly cooled to room temperature. Judging from the WAXD patterns recorded on photographic films, the particular molecular orientations pre-existing in the pellets seemed to be successfully removed by these processes. Then both specimens were subjected to WAXD measurements at 150, 180, 210, 240, 270 and 300°C by raising the temperature stepwise. The WAXD profiles of the PET and X-7G specimens are shown in *Figure 1* as a function of temperature.

In contrast to the well-developed crystalline diffraction peaks in the WAXD profiles of PET shown in *Figure 1a*, the peaks for X-7G in *Figure 1b* are quite few and small. Moreover, none of the scattering angles (2θ) of the diffraction peaks of X-7G coincide with those of PET, suggesting that the PET sequences in X-7G did not crystallize. The sharp diffraction peak observed at $2\theta = 19.7°$ (Bragg spacing $d_{\text{Bragg}} = 0.45$ nm) can be attributed to the crystals of the OBA sequences of X-7G[10,14,50]. The subsidiary peak at $\theta = 23.1°$C ($d_{\text{Bragg}} = 0.38$ nm) may also come from the intramolecular atomic order of the OBA sequences[11,14]. From a series of diffraction profiles for X-7G measured at 210°C < T < 240°C, its melting point can be approximately ascertained as 233°C, at which the diffraction peak of the OBA crystals at $2\theta \approx 20°$ completely disappears. The melting temperature of PET was determined as about 270°C, at which all diffraction peaks relevant to PET crystals essentially disappear. The glass transition temperatures, the temperatures of crystallization from the glassy state and the melting temperatures of X-7G and PET were also measured by d.s.c.

We summarize and define the transition temperatures measured in this study and reported elsewhere[1,24] as follows: $T_{\text{m,X-7G}}$(≈ 233°C) is the melting temperature of

X-7G, $T_{g,X\text{-}7G}^{PET}(\approx 120°C)$ is the glass transition temperature of the sequences rich in PET segments in X-7G and $T_{g,X\text{-}7G}^{OBA}(\approx 170°C)$ is the glass transition temperature of the sequences rich in OBA segments in X-7G. We also define $T_{m,PET}(\approx 270°C)$, $T_{c,PET}^{max}(\approx 160°C)$ and $T_{g,PET}(\approx 80°C)$ as the melting temperature, the temperature at which crystallization from the glassy state occurs at a maximum rate and the glass transition temperature of PET, respectively. Finally, we define $T_{NN\rightarrow NI}$ as the transition temperature from the pure nematic LC state to the biphasic state of X-7G within which the anisotropic and isotropic liquid phases coexist[19]. It should be noted that the transition temperatures reported here (in *Figure 2*) for X-7G should strongly depend on the thermal history of the specimens used for the experiments and that they are not necessarily identical to those expected for the X-7G specimens prepared by the rapid solution-casting method used in this work. The results summarized in *Figure 2*, however, still provide important information to allow interpretation of their influences on the phase separation of mixtures.

Formation of the phase-separated structure as observed with the PLM

Here we present our real-time and *in-situ* observations concerning the formation of the phase-separated structure in the isothermal phase separation of the mixtures and the nematic ordering process, i.e. the annihilation of disclinations in the LC domains. Observations were made by means of the PLM as the specimens were subjected to rapid T-jumps to various annealing temperatures. In order to understand qualitatively the influence of all the factors such as glass transition, crystallization, melting and degradation on the phase-separated structure, it is important to observe the phase separation process of the mixture and the nematic ordering process in the LC domains over a wide temperature range. Micrographs of the mixture specimens subjected to T-jumps at 12 different annealing temperatures between 25 and 400°C were taken under crossed polarizers and a red retardation plate as a function of annealing time. Five of them obtained at 140, 230, 240, 280 and 380°C are shown in *Figure 3*. The corresponding annealing times are indicated on the micrographs. At each temperature, a series of micrographs were taken for the same area of the same specimen. The orientations of the polarizer (P), analyser (A) and red plate (R) are indicated in *Figure 3*. Because the red plate was inserted between the crossed polarizers, the isotropic domains normally appeared red and the anisotropic domains exhibited different colours such as green, blue or yellow, depending partially on the relative orientation between the retardation direction of the red plate and the direction of the molecular director. The micrographs in *Figure 3* (and the others not shown here) for different annealing temperatures and different annealing times clearly demonstrate the significant dependence of the evolution of the phase-separated structure and the nematic ordering process in the LC domains on the annealing temperature.

At temperatures below 80°C ($T_{g,PET}$) (regime I in *Figure 2*), no significant phase-separated structure appears, indicating that the system maintains the frozen-in homogeneous structure produced by the special sample preparation technique. At 80°C < T < 170°C ($T_{g,X\text{-}7G}^{OBA}$)

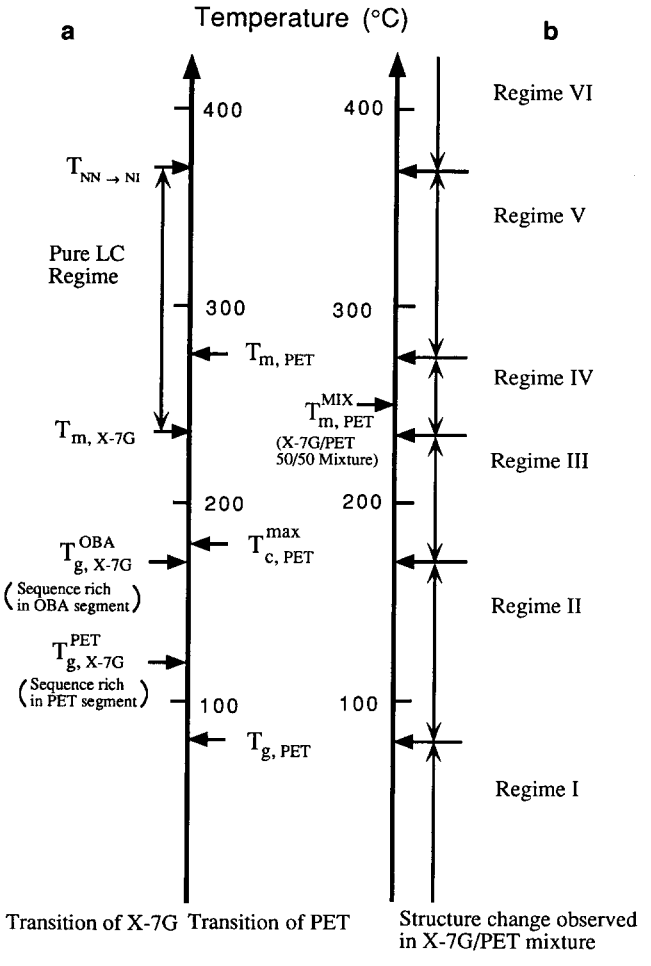

Figure 2 The various transition temperatures, such as T_g, T_c (crystallization temperature) and T_m, of neat X-7G and neat PET (a) and their influences on the ordering processes of the X-7G/PET mixture (b). The ordering process observed in each regime is described in the text

(regime II in *Figure 2*), very small anisotropic domains with yellow or blue colour (which may have been the anisotropic LC domains of X-7G and/or the crystallites of PET) started to form in the red isotropic matrix (which may have been the amorphous domains of PET and/or X-7G) (see the data taken at 140°C). These domains, however, did not grow further with time, indicating that above $T_{g,PET}$ the phase separation seems to start but is pinned immediately after the onset of phase separation. The pinning effect may be due to crystallization of PET and/or vitrification of X-7G. In fact, in our d.s.c. measurements we observed that the glass transition temperature of the OBA-rich component in X-7G ($T_{g,X\text{-}7G}^{OBA}$) is 170°C and the onset temperature of crystallization for amorphous PET from the glassy state is 134°C. An increase in the local concentration of X-7G due to phase separation increases the local anisotropy but at the same time it increases the local glass transition temperature, resulting in a freezing in of the molecular motion and further growth of the domain structure. Similarly, an increase in the local concentration of PET induces crystallization of PET, giving rise to anisotropic structures. This may also obstruct further development of the phase-separated structure.

When the annealing temperature was higher than

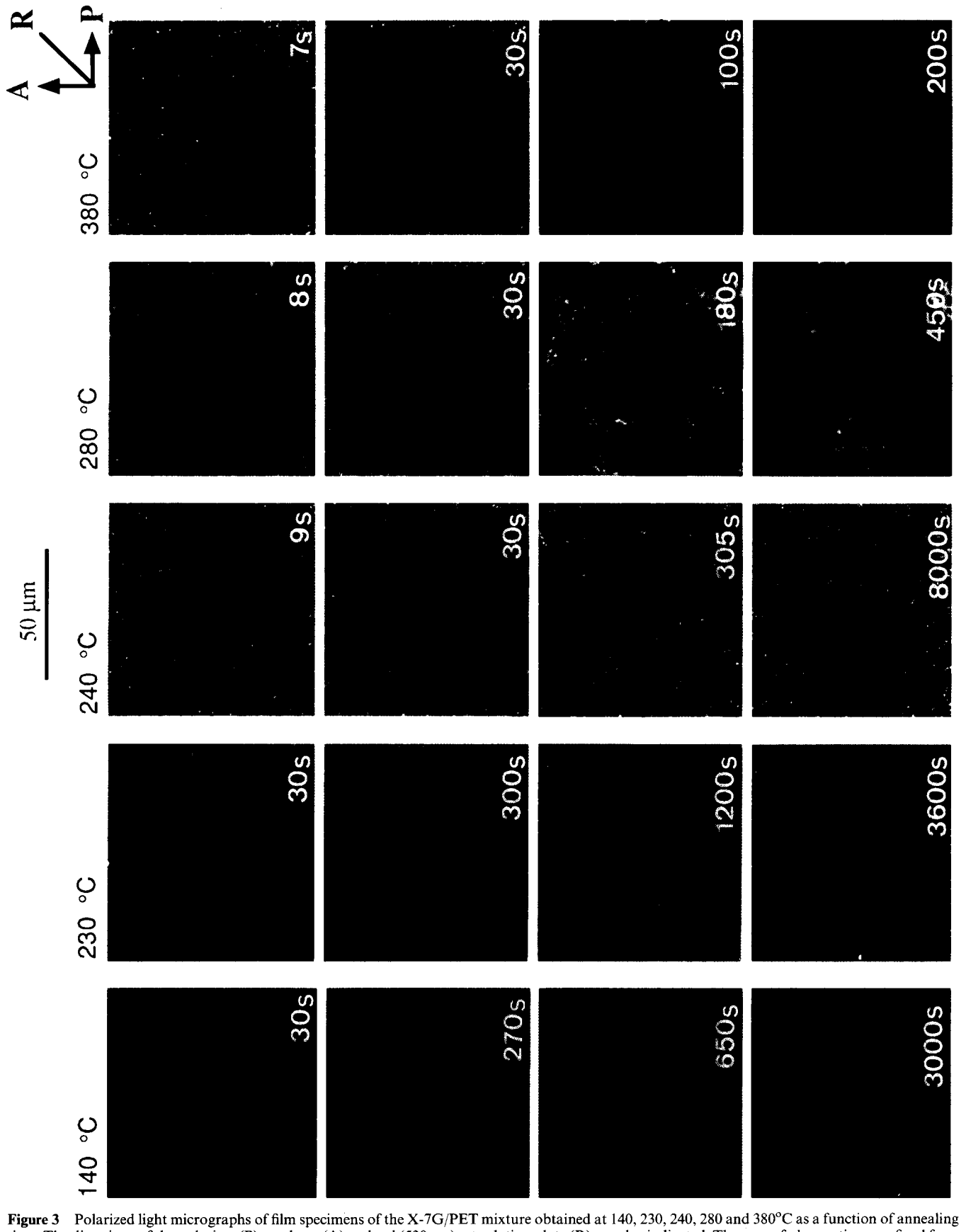

Figure 3 Polarized light micrographs of film specimens of the X-7G/PET mixture obtained at 140, 230, 240, 280 and 380°C as a function of annealing time. The directions of the polarizer (P), analyser (A) and red (530 nm) retardation plate (R) are also indicated. The area of observation was fixed for a given temperature

170°C but lower than $T_{m,X\text{-}7G}(\approx 233°C)$ (regime III in *Figure 2*), for instance, at 230°C, we observed that within the first few seconds the whole specimen transformed from the isotropic state to the anisotropic state and then small isotropic droplets (rich in PET) with red colour appeared. However, the anisotropic area (rich in X-7G) with yellow or blue colour seen on the micrographs in the second column of *Figure 3* is somewhat different in brightness and colour compared to the anisotropic area observed at higher temperatures, such as 240 and 280°C, where complete phase separation occurred, as will be shown later. It is difficult to define the boundary between the anisotropic and isotropic domains. The LC texture within the anisotropic domains is not clear. The average size of the isotropic domains is in the range of 1–2 μm. During annealing at 230°C, no further growth of the phase-separated domains could be detected. These results imply that the crystallization of the pure PET or OBA units of X-7G in the mixture prevents growth of the phase-separated domains, because the large scale translational diffusion of the molecules required for the development of phase separation and coarsening of the phase-separated structure is hindered or suppressed by the crystallization of pure PET or OBA sequences in X-7G. Although the experimental data are not shown in this paper, we confirmed the diffraction peaks corresponding to both X-7G and PET crystals in the WAXD profile of the X-7G/PET mixture obtained at 150°C. Those peaks had mostly disappeared in the WAXD profile obtained at 260°C.

When the annealing temperature was higher than $T_{m,X\text{-}7G}$ but lower than $T_{m,PET}(\approx 270°C)$ (regime IV in *Figure 2*), for instance, at 240°C, unmixing between X-7G and PET rapidly occurred, as shown by the micrographs in the third column of *Figure 3*. The micrograph taken at 9 s after the T-jump to 240°C clearly shows the phase-separated structure composed of optically anisotropic domains (i.e. an anisotropic liquid of X-7G, distinguished by the yellow and blue areas on the micrograph) and isotropic domains (i.e. an isotropic melt of PET, distinguished by the red areas on the micrograph). On this micrograph we can see distinct boundaries between anisotropic and isotropic domains. At 30 s, a well-defined phase-separated structure can be seen. It corresponds to the structure developed in the late stage SD where the local compositions of the phases reach the equilibrium compositions determined from the phase diagram of the mixture, and the domains grow further with dynamic self-similarity (see elsewhere[51,52] for a definition of the late stage SD). Moreover, each phase has an area fraction of 0.5, equal to the initial volume fraction of each component in the mixture. These results may simply imply that the phase separation develops bicontinuous domains composed of almost pure PET (isotropic domains) and X-7G (anisotropic domains) and that the three-dimensional domain structure rapidly reaches the two-dimensional one because the characteristic length of the domains rapidly increases and exceeds the thickness of the film. The brightness and colour of the anisotropic domains on the micrographs taken at 240°C are different from those on the micrographs taken at 230°C. Within the anisotropic domains a certain liquid crystalline texture has been formed, but we cannot identify the kind of texture. In this study we will call it an 'ill-defined texture'.

Coarsening of the phase-separated structure continues for a while at 240°C but seems to stop at about 300 s, which can be deduced from the fact that the phase-separated image on the micrograph taken at 305 s did not change even after 8000 s. Here it is important to note that the effective melting temperature of the PET component in the mixture ($T_{m,PET}^{MIX}$) is generally lower than that of neat PET ($T_{m,PET}$) owing to the melting point depression effect[53]. $T_{m,PET}^{MIX}$ increases with time during the course of phase separation because the local content of PET in the PET-rich phase increases with time until the equilibrium compositions are reached. When $T_{m,PET}^{MIX}$ exceeds the annealing temperature, the crystallization of the PET component starts to occur locally. Upon the completion of phase separation, the PET phase gradually crystallizes and structural growth is eventually pinned down. Thus, for an annealing temperature lower than 270°C ($T_{m,PET}$), pinning of the growth of the phase-separated domain structure due to crystallization of the PET component was observed. The PET crystallites formed during phase separation may be very small as they could not be observed with the PLM.

At $T_{m,PET} \leq T \leq T_{NN\rightarrow NI}(\approx 370°C)$ (regime V in *Figure 2*), phase separation and the coarsening process of the phase-separated structure occur very rapidly. An example is shown by the series of micrographs taken at 280°C in the fourth column of *Figure 3*, in which the red phase is isotropic liquid and the phase having green and blue retardation colours consists of anisotropic liquid. After 8 s from the T-jump, the network structure of the anisotropic phase is already formed. Both anisotropic and isotropic phases have a volume fraction of 0.5, corresponding to the initial composition of the mixture. This probably indicates that each phase consists of almost pure X-7G or PET. As the annealing time elapses, the domain structure rapidly changes from three-dimensional to two-dimensional. The optically anisotropic network structure was rapidly coarsened mainly by the disruption of the network (see the difference between the images at 8 and 30 s). Finally, the global continuity of the network was disrupted to result in the formation of anisotropic fragments. These anisotropic fragments shrank into the droplets in order to reduce the interfacial area (and hence the interfacial free energy) between the anisotropic and isotropic phases. The process followed was a diffusional coalescence of these anisotropic droplets to form larger domains. The mechanisms of phase separation and the coarsening process in this temperature range will be discussed in detail elsewhere[46].

At $T > T_{NN\rightarrow NI}$ (regime VI in *Figure 2*), for instance, at 380°C, chemical degradation of the two components, transesterification and the biphasic characteristics of X-7G itself[19] result in the disappearance of anisotropic domains shortly after phase separation. At this temperature the anisotropic domains almost disappear from view after about 200 s from the T-jump, as shown by the micrographs in the last column of *Figure 3*.

From the features of the phase-separated structure, we can define the following six temperature regimes, as shown in *Figure 2*, within the temperature range covered in this study. In regime I, $T < T_{g,PET}(\approx 80°C)$, the system maintains the frozen-in homogeneous state formed in the particular preparation process of the specimens. In regime II,

$T_{g,PET} < T < T^{OBA}_{g,X\text{-}7G} (\approx 170°C)$, unmixing stops at a very early stage of the SD owing to the vitrification of X-7G and/or the crystallization of PET. In regime III, $T^{OBA}_{g,X\text{-}7G} < T < T_{m,X\text{-}7G} (\approx 233°C)$, unmixing stops in the middle of the SD owing to the crystallization of X-7G and/or PET before coarsening occurs. In regime IV, $T_{m,X\text{-}7G} < T < T_{m,PET} (\approx 270°C)$, pinning of the phase-separated structure occurs during the coarsening process in the later stages of the SD owing to the crystallization of PET. In regime V, $T_{m,PET} < T < T_{NN \rightarrow NI} (\approx 370°C)$, phase separation and coarsening occur rapidly and continue without pinning, so that only the late stage SD can be observed over the time scale covered in this experiment. Finally, in regime VI, $T > T_{NN \rightarrow NI}$, chemical degradation, transesterification and the biphasic nature of X-7G result in the disappearance of the anisotropic domains.

The transesterifiction reaction in the mixture was investigated and is reported in detail elsewhere[46]. Here, it may be appropriate to mention in short that the transesterification reaction is not significant at a temperature below 270°C.

Phase-separated structure as observed by LS

We first define the coordinate system for our light-scattering experiments, as shown in *Figure 4*. *OXYZ* is the Cartesian coordinate system fixed to the laboratory. *OX* is the propagation direction of the incident laser beam. The scattering intensity was recorded as a function of the scattering angle θ and azimuthal angle μ with a two-dimensional detector (photographic plate) placed normal to the *OX* axis (or parallel to the *YZ* plane). The terms $\mathbf{s}_0$ and $\mathbf{s}$ denote the unit vectors parallel to the propagation directions of the incident beam and the scattered light, respectively.

Figure 5 shows the evolution with time of the light-scattering patterns of the mixture obtained for the V_V condition (*Figure 5a*) and the corresponding PLM micrographs (*Figure 5b*) obtained from the early period of the late stage SD during the isothermal phase separation at 270°C (regime IV). The orientations of the polarizer and analyser and the annealing times are indicated in the figure. The ring-like scattering patterns correspond to the 'spinodal rings' observed for critical mixtures of binary liquid polymers in the unmixing process[54]. The peak position shifts with annealing time towards the incident beam axis; that is, the scattering angle at maximum intensity (θ_{max}) decreases with time. This is consistent with evolution with time of the corresponding domain structure observed in the PLM images, indicating growth of the characteristic length for the periodic concentration fluctuations originating from the spinodal decomposition. This length should be essentially identical to that for the periodic fluctuations in optical anisotropy. The effect of one phase consisting of an anisotropic liquid on the scattering patterns will be discussed below.

Figure 5 also shows the influence of the orientation order parameter on the scattering patterns: the scattering intensity along the equator is significantly stronger thanthat along the meridian, leading to a scattering pattern with a two-half-moon (or two-crescent-moon) shape along the equator for the V_V condition, i.e. the intensity distribution depends upon the azimuthal angle μ. The influence of the orientation order parameter

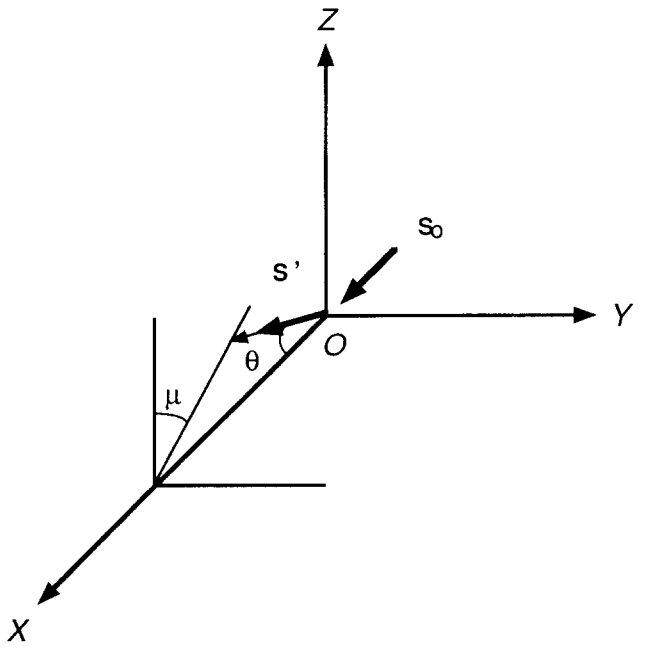

Figure 4 Coordinate system *OXYZ* fixed to the laboratory. The terms $\mathbf{s}_0$ and $\mathbf{s}$ are unit vectors along the incident and scattering beams; θ and μ are the scattering angle and the azimuthal angle, respectively

on the scattering patterns can also be seen in *Figure 6*, which shows three scattering patterns obtained for the H_V, V_V and H_H conditions from film specimens isothermally annealed at 238°C (regime IV) for 8 s and then quenched to room temperature. These characteristics concerning the anisotropy in the scattering intensity distribution, i.e. the μ-dependent intensity distribution, are related to the anisotropic nature of LC domains in this system and can never be observed in a multiphase system composed of only amorphous polymers. We will analyse these scattering patterns in the next section.

The influence of the concentration order parameter on the scattering patterns is demonstrated in *Figure 7*. The micrographs shown here are the ones produced after binarization of the PLM images[46]. All information related to the orientation order parameter and the orientation fluctuations associated with the defects in the anisotropic domains has been erased in the binarization process, as shown by the three micrographs in *Figure 7a*. The bright and dark areas on the micrographs only represent the local variations of the concentration order parameter, i.e. the local differences in the concentration of PET and X-7G. The corresponding optical diffraction patterns in *Figure 7b* show the real 'spinodal rings' only relevant to the concentration fluctuations, i.e. they are independent of the azimuthal angle μ. The characteristic lengths as determined from the optical diffraction patterns and their evolution with time are consistent with those directly obtained by the light-scattering method. These analyses indicate that the spatial variations of both the concentration and orientation order parameters in the X-7G/PET two-phase system are identical, causing a scattering ring located at the same scattering angle, i.e. the length scale of the concentration fluctuations is the same as that of the orientation fluctuations in this system.

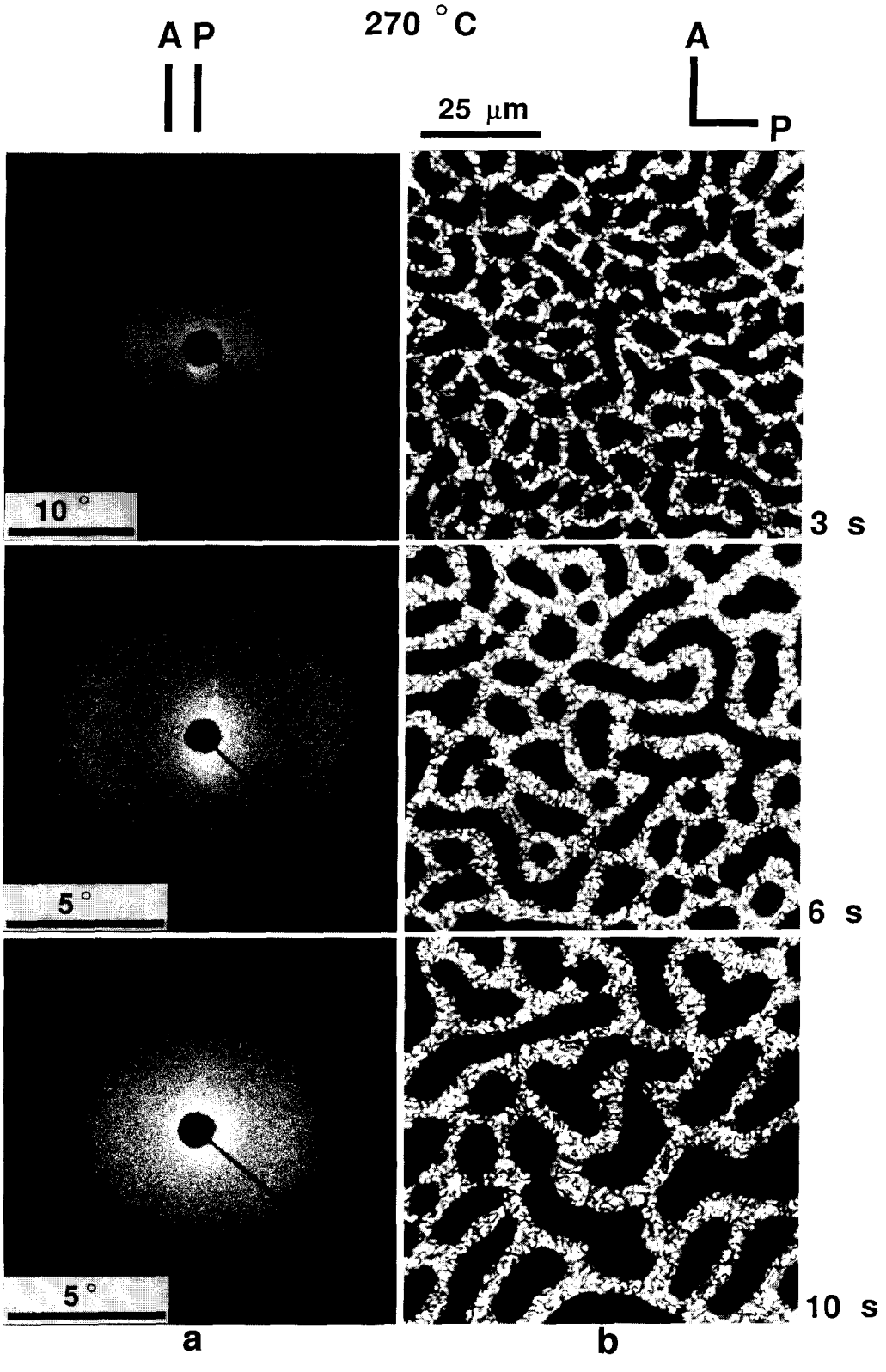

Figure 5 Light-scattering patterns (a) obtained under the V_V condition and the corresponding polarized light micrographs (b) for the X-7G/PET specimens annealed at 270°C for 3, 6 and 10 s. The orientations of the polarizers (P) and the analysers (A) are also indicated

Origin of the azimuthal angle dependent scattering patterns: orientation and concentration order parameters

The two-phase structure shown in *Figure 5* was found to give unique H_V, V_V and H_H small-angle light-scattering patterns, as shown in *Figure 6*. Under the H_V condition, a four-fold symmetry pattern with the intensity maxima at odd multiples of the azimuthal angle ($\mu = 45°$) is observed. Under the V_V condition, a pattern with two-fold symmetry having two strong intensity maxima at $\mu = 90$ and 270° and two weak intensity maxima at $\mu = 0$ and 180° is observed. The scattering pattern obtained under the H_H condition exhibiting two

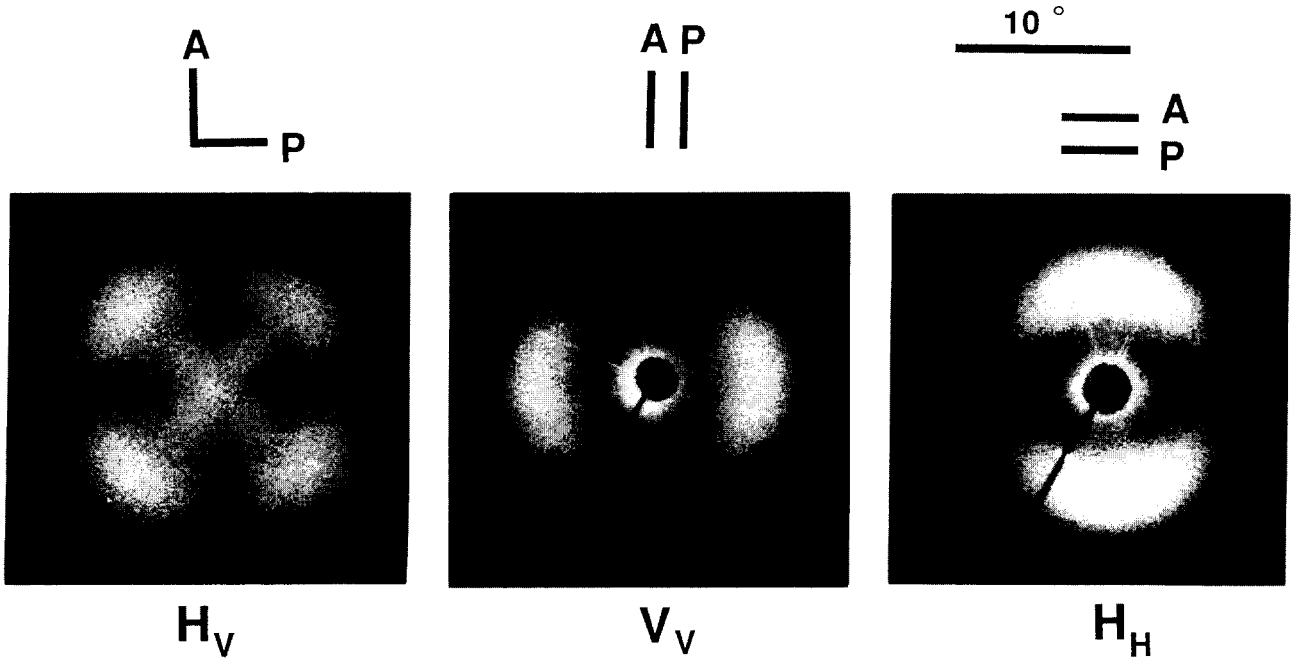

Figure 6 Light-scattering patterns obtained under H_V, V_V and H_H conditions from a specimen of the X-7G/PET mixture annealed at 238°C for 8 s. The orientations of the polarizers (P) and the analysers (A) are also indicated

strong intensity maxima on the meridian ($\mu = 0$ and 180°) is identical to that obtained under the V_V condition if it is rotated by 90°. Comparing the three scattering patterns in *Figure 6*, we can see that the scattering angle (θ_{max}) of the intensity maximum is independent of the orientations of the polarizer and analyser, i.e. the H_V, V_V and H_H scattering patterns give the same θ_{max} value. The angle θ_{max} is also independent of μ under any given polarization conditions. The μ dependence of the scattering patterns varies only with the polarization condition but not with annealing time. However, θ_{max} shifts with annealing time towards the incident beam axis owing to coarsening of the two-phase structure at $T \geq T_{m,PET}$.

Let us consider the origin of such an anisotropic scattering pattern. The scattering element as schematically shown in *Figure 8a* approximately has a uniaxial anisotropy with its polarizabilities α_1 parallel to the principal optical axis and α_2 perpendicular to this axis. For X-7G, the anisotropic phase may have $\alpha_1 \gg \alpha_2$. The principal optical axis of the scattering element is indicated by the unit vector **d**, and **e** is the unit vector parallel to the polarizer. The micrographs in *Figure 5* show that there are various kinds of defects in the anisotropic domains, giving rise to a schlieren texture. Those defects cause an orientation distribution of the principal optical axes of the scattering elements, as depicted by those axes with vectors $\mathbf{d}_i (i = 1, 2, 3, \ldots)$ for the ith element in *Figure 8b*. The orientation distribution of $\mathbf{d}_i$ in the anisotropic domain may have uniaxial symmetry around the director **m** of the network of the anisotropic domain. We define β as the polar angle between **m** and **d**, and $\alpha_{\|}$ and $\alpha_{\perp}$ as the polarizabilities parallel and perpendicular to **m**, respectively. The anisotropic domains are surrounded by isotropic domains with polarizability α_S. The optical anisotropy of the anisotropic network ($\alpha_{\|} - \alpha_{\perp}$) can be related to the intrinsic anisotropy of the element ($\alpha_1 - \alpha_2$) by

$$\alpha_{\|} - \alpha_{\perp} = (\alpha_1 - \alpha_2)\frac{3\langle\cos^2\beta\rangle - 1}{2} \quad (1)$$

Figure 9 shows the orientations of an anisotropic domain with director **m** under the V_V and H_V conditions. As illustrated in *Figure 9a* for the V_V condition, the polarization directions of the polarizer (P) and the analyser (A), are parallel to the unit vector **k** along the *OZ* axis defined in *Figure 4*. The angle between the director **m** and the polarizer is defined as α. Under the H_V condition, P is parallel to **k** and A is parallel to the unit vector **j** along the *OY* axis, as illustrated in *Figure 9b*. Under the H_H condition, both P and A are parallel to **j**. Hereafter, we define **M** as the dipole moment induced by the electric field of the incident light in the volume element and **O** as the unit vector in the polarization direction of the analyser. For the V_V scattering pattern the induced dipole moment $(\mathbf{M}\cdot\mathbf{O})_{V_V}$ is given by

$$\begin{aligned}(\mathbf{M}\cdot\mathbf{O})_{V_V} &= \mathbf{M}_V \cdot \mathbf{O}_V = E_0[\delta(\mathbf{k}\cdot\mathbf{m})\mathbf{m} + b_t\mathbf{k}]\cdot\mathbf{k} \\ &= E_0[\delta(\mathbf{k}\cdot\mathbf{m})^2 + b_t] \\ &= E_0[(\alpha_{\|} - \alpha_{\perp})\cos^2\alpha + (\alpha_{\perp} - \alpha_S)] \quad (2)\end{aligned}$$

where $b_t = \alpha_{\perp} - \alpha_S$, $\delta = \alpha_{\|} - \alpha_{\perp}$ and E_0 is the electric field strength of the incident beam. $\mathbf{M}_V$ and $\mathbf{O}_V$ are respectively the induced dipole moment for the vertically polarized incident beam and the unit vector in the polarization direction of the analyser under the V_V condition. The term $(\alpha_{\|} - \alpha_{\perp})\cos^2\alpha$ indicates the influence of the orientation order parameter on the scattering intensity and gives rise to the μ dependence in the V_V pattern. The term $\alpha_{\perp} - \alpha_S$ indicates the influence of the concentration order parameter on the scattering intensity and is μ independent.

If the system studied satisfies the criteria $\alpha_{\|} - \alpha_{\perp} > 0$ in the anisotropic domain, $\alpha_{\perp} - \alpha_S > 0$ between

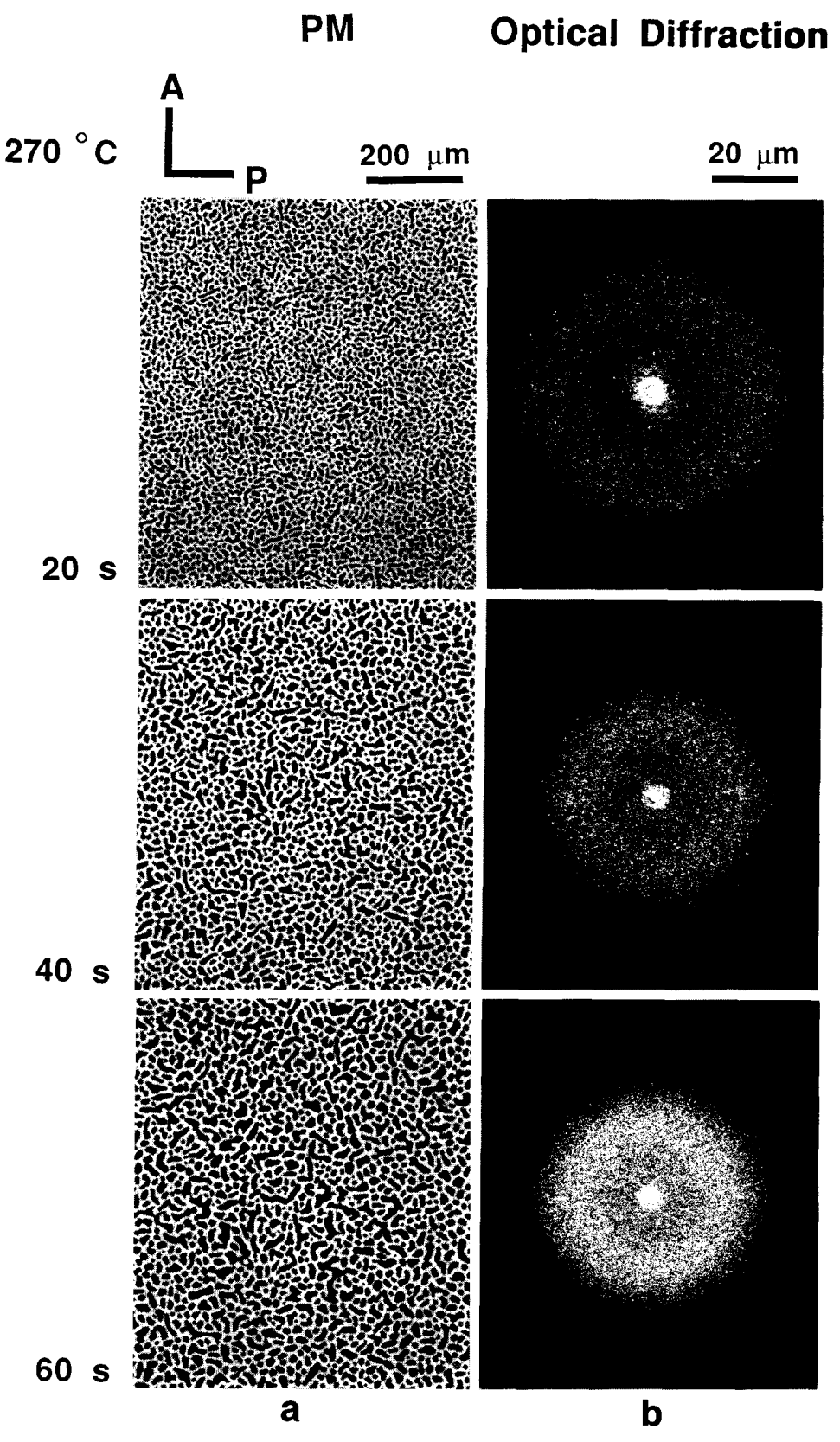

Figure 7 Binarized polarized light micrographs of the X-7G/PET mixture obtained *in situ* at 270°C after 20, 40 and 60 s of the temperature jump (a) and the corresponding optical Fourier transformations (b)

the anisotropic and isotropic domains, and $\alpha_{\parallel} - \alpha_{\perp} \gg \alpha_{\perp} - \alpha_S$ because of the strong anisotropy in the anisotropic domain, maxima for $(\mathbf{M} \cdot \mathbf{O})_{V_v}$ appear at $\alpha = 0$ and 180°. Thus, in this case the anisotropic domains with their directors **m** oriented parallel to **k** (the *OZ* axis) make the largest contribution to the V_V scattering intensity. The V_V scattering intensity is generally given as

$$\mathbf{I}_{V_v} \approx | \mathcal{F}\{(\mathbf{M} \cdot \mathbf{O})_{V_v}\} |^2 \quad (3)$$

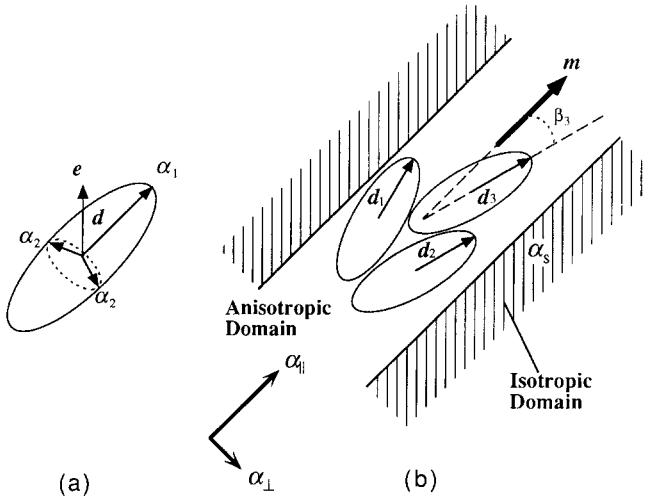

Figure 8 (a) A schematic representation of a scattering volume element with the principal optical axis denoted by the unit vector **d** and the polarizabilities α_1 parallel to **d** and α_2 perpendicular to **d**. The term **e** is the unit vector parallel to the electric vector of the polarizer. (b) A model of a long anisotropic domain composed of the elements formed during phase separation. The terms $\alpha_{\parallel}$ and $\alpha_{\perp}$ are the polarizabilities parallel and perpendicular to the principal axis of the anisotropic domain denoted by the unit vector **m**

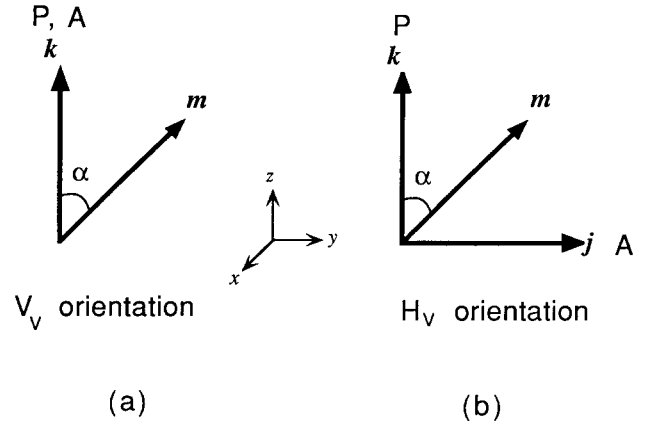

Figure 9 Orientations of polarizers (P) and analysers (A) in the V_V (a) and H_V (b) conditions. The unit vector **m** denotes the principal optical axis (director) of the anisotropic domain, and α is the angle between m and the direction of the polarizer

where $\mathcal{F}$ designates the Fourier transformation of the spatial variation of $(\mathbf{M}\cdot\mathbf{O})_{V_v}$. The V_V scattering pattern and the anisotropic domains which give the largest contribution to the V_V scattering are schematically represented in *Figure 10a*. In this case the maxima of the scattering intensity will appear at $\mu = 90$ and 270°. On the other hand, the minima will appear at $\mu = 0$ and 180°, as shown in *Figure 10b*. In *Figure 10*, q_{max} is the magnitude of the scattering vector at the maximum scattering intensity and is defined by

$$q_{max} = \frac{4\pi}{\lambda} \sin \frac{\theta_{max}}{2} \tag{4}$$

where θ_{max} is the scattering angle at the maximum intensity and λ is the wavelength of the incident beam, both in the medium. Also q_{max} is related to the

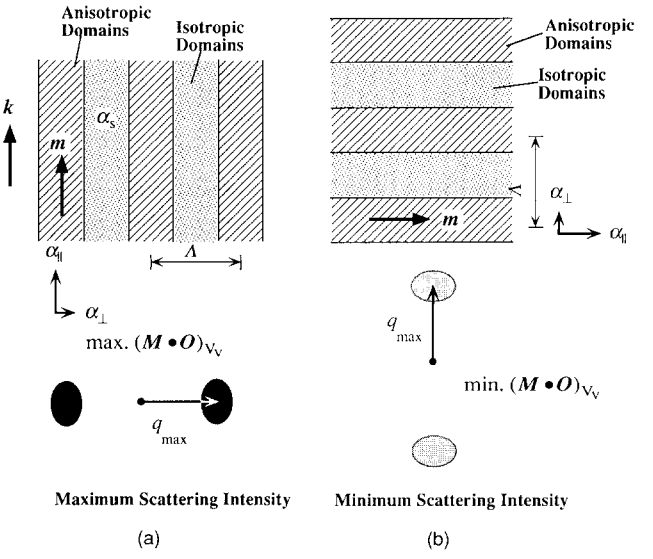

Figure 10 Schematic diagrams indicating the orientations of the anisotropic domains and the corresponding V_v scattering patterns: the conditions for maximum (a) and minimum (b) scattering intensities

average spacing Λ of the anisotropic domains by $q_{max} = 2\pi/\Lambda$.

For the H_V scattering pattern, the induced dipole moment $(\mathbf{M}\cdot\mathbf{O})_{H_v}$ is given by

$$\begin{aligned}(\mathbf{M}\cdot\mathbf{O})_{H_v} &= \mathbf{M}_V\cdot\mathbf{O}_H = E_0[\delta(\mathbf{k}\cdot\mathbf{m})\mathbf{m} + b_t\mathbf{k}]\cdot\mathbf{j} \\ &= E_0\delta(\mathbf{k}\cdot\mathbf{m})(\mathbf{j}\cdot\mathbf{m}) \\ &= E_0(\alpha_{\parallel} - \alpha_{\perp})\cos\alpha\,\sin\alpha \end{aligned} \tag{5}$$

where $\mathbf{O}_H$ is the unit vector in the polarization direction of the analyser under the H_V condition. Obviously, the term $\alpha_{\perp} - \alpha_S$ or $\alpha_{\parallel} - \alpha_S$, related to the concentration order parameter, does not appear in equation (5). The term $|(\mathbf{M}\cdot\mathbf{O})_{H_v}|$ becomes a maximum at odd multiples of $\alpha = 45°$. Therefore, the intensity maxima appear at odd multiples of $\mu = 45°$, resulting in a scattering pattern with four-fold symmetry, as seen in *Figure 6*.

For the H_H scattering pattern, the induced dipole moment $(\mathbf{M}\cdot\mathbf{O})_{H_H}$ is given by

$$\begin{aligned}(\mathbf{M}\cdot\mathbf{O})_{H_H} &= \mathbf{M}_H\cdot\mathbf{O}_H = E_0[\delta(\mathbf{j}\cdot\mathbf{m})\mathbf{m} + b_t\mathbf{j}]\cdot\mathbf{j} \\ &= E_0[\delta(\mathbf{j}\cdot\mathbf{m})^2 + b_t] \\ &= E_0[(\alpha_{\parallel} - \alpha_{\perp})\sin^2\alpha + (\alpha_{\perp} - \alpha_S)] \end{aligned} \tag{6}$$

where $\mathbf{M}_H$ is the induced dipole moment for the horizontally polarized incident beam. Comparing equation (6) with equation (2), we can see that the term $(\alpha_{\parallel} - \alpha_{\perp})\sin^2\alpha$ in equation (6) is different from the term $(\alpha_{\parallel} - \alpha_{\perp})\cos^2\alpha$ in equation (2). Clearly, the scattering intensity distribution under the H_H condition is similar to that obtained under the V_V condition except for the fact that the intensity maxima of the H_H pattern should appear on the meridian, i.e. at $\mu = 0$ and 180°, instead of $\mu = 90$ and 270°.

LC effect

Earlier, we showed evidence of the rapid phase separation at $T > T_{m,X\text{-}7G}$ (i.e. in regimes IV and V in *Figure 2*): within a few seconds, we obtained the

phase-separated structure corresponding to the late stage SD. The rapid phase separation may be closely related to one of the phases (X-7G) being able to form a liquid crystal.

The molecular weights of the X-7G and PET used are relatively low, so that the mixture has high mobility and hence a high rate of domain growth. Moreover, the LC nature of the X-7G phase further reduces the viscosity of the X-7G phase and hence increases the growth rate of the domains.

For a polymer mixture with one component being an LC polymer, the difference in chain stiffness and anisotropic segmental interactions have to be taken into account[43–45]. The anisotropic segmental interactions cause the semiflexible chains to self-assemble and hence form the pure LC phase, enhancing the segregation power between the semiflexible and flexible chains to a great extent. Thus, the enhanced segregation power arising from the effect of one component being an LC polymer further increases the thermodynamic driving force for phase segregation and hence the growth rate of the domains.

CONCLUSIONS

The experimental results on the two-phase structures formed by phase separation via spinodal decomposition in the X-7G/PET mixture show that the vitrification and crystallization of PET and/or X-7G can pin the growth of the structure at different stages of the SD, i.e. the formation of two-phase structures is strongly dependent upon the isothermal annealing temperature. At $T < T_{g,PET}$, the system maintains the frozen-in homogeneous structure formed in the particular preparation process of the specimens. At $T_{g,PET} < T < T_{g,X\text{-}7G}^{OBA}$, unmixing is pinned by the vitrification of X-7G and/or the crystallization of PET in the very early stage SD, and at $T_{g,X\text{-}7G}^{OBA} < T < T_{m,X\text{-}7G}$, unmixing is pinned by the crystallization of X-7G and/or PET in the middle stage SD. At $T_{m,X\text{-}7G} < T < T_{m,PET}$, the coarsening process is pinned by the crystallization of PET in the late stage SD. At $T_{m,PET} < T < T_{NN \rightarrow NI}$, phase separation and coarsening occur rapidly without pinning. The rapid phase separation at $T > T_{m,X\text{-}7G}$ may be closely related to the nature of the X-7G phase, i.e. a relatively low viscosity and anisotropic segmental interactions.

The theoretical analysis concerning the polarized or depolarized light-scattering patterns indicates that the V_V and H_H scattering patterns depend upon both the orientation and concentration order parameters, while the H_V scattering patterns depend only upon the orientation order parameter. The orientation and concentration order parameters, respectively, give μ dependent and μ independent scattering patterns. The fact that the V_V and H_V scattering patterns depend upon μ indicates that the contribution of the orientation order parameter to the scattering is greater than that of the concentration order parameter. In the system we studied, however, the characteristic length scales for the concentration and orientation order parameters were essentially identical.

ACKNOWLEDGEMENT

We thank Professor Masaki Tsuji of the Chemical Institute, Kyoto University, for helping in the optical diffraction measurements.

REFERENCES

1 Jackson, W. J. and Kuhfuss, H. F. *J. Polym. Sci., Polym. Chem. Edn* 1976, **14,** 2043
2 McFarlane, F. E., Nicely, V. A. and Davis, T. G. in 'Contemporary Topics in Polymer Science' (Eds E. M. Pearce and J. R. Schaefgen), Vol. 2, Plenum Press, New York, 1977, p. 109
3 Calundann, G. W. *US Pat. 4 161 470* 1980
4 Acierno, D., LaMantia, F. P., Polizzotti, G., Ceferri, A. and Valenti, B. *Macromolecules* 1982, **15,** 1455
5 Sugiyama, H., Lewis, D. N., White, J. L. and Fellers, J. L. *J. Appl. Polym. Sci.* 1985, **30,** 2329
6 Benson, R. S. and Lewis, D. N. *Polym. Commun.* 1987, **28,** 289
7 Kalika, D. S., Giles, D. W. and Denn, M. M. *J. Rheol.* 1990, **34,** 139
8 Cocchini, F., Nobile, M. R. and Acierno, D. *J. Rheol.* 1991, **35,** 1171
9 Mackley, M. R., Pinuad, F. and Siekmann, G. *Polymer* 1981, **22,** 437
10 Zachariades, A. E., Economy, J. and Logan, J. A. *J. Appl. Polym. Sci.* 1982, **27,** 2009
11 Mitchell, G. R. and Windle, A. H. *Polymer* 1982, **23,** 1269
12 Viney, C., Mitchell, G. R. and Windle, A. H. *Polym. Commun.* 1983, **24,** 145
13 Mitchell, G. R. and Windle, A. H. *Polymer* 1983, **24,** 1513
14 Blackwell, J. D., Lieser, G. and Gutierrez, A. H. *Macromolecules* 1983, **16,** 1418.
15 Joseph, E. G., Wilkes, G. L. and Baird, D. G. *Polymer* 1985, **26,** 689
16 Joseph, E. G., Wilkes, G. L. and Baird, D. G. *Polym. Eng. Sci.* 1985, **25,** 377
17 Viney, C., Donald, A. M. and Windle, A. H. *Polymer* 1985, **26,** 870
18 Shiwaku, T., Nakai, A., Hasegawa, H. and Hashimoto, T. *Polym. Commun.* 1987, **28,** 174
19 Shiwaku, T., Nakai, A., Hasegawa, H. and Hashimoto, T. *Macromolecules* 1990, **23,** 1590
20 Spontak, R. J., Windle, A. H. and MacDonald, W. A. *J. Mater. Sci.* 1991, **26,** 4234
21 Hudson, S. D. and Lovinger, A. J. *Polymer* 1993, **34,** 1123
22 Lader, H. J. and Krigbaum, W. R. *J. Polym. Sci., Polym. Phys. Edn* 1979, **17,** 1661
23 Menczel, J. and Wunderlich, B. *J. Polym. Sci., Polym. Phys. Edn* 1980, **18,** 1433
24 Meesiri, W., Menczel, J., Gaur, U. and Wunderlich, B. *J. Polym. Sci., Polym. Phys. Edn* 1982, **20,** 719
25 Viney, C. and Windle, A. H. *J. Mater. Sci.* 1982, **17,** 2661
26 Nicely, V. A., Dougherty, J. T. and Renfro, L. W. *Macromolecules* 1987, **20,** 573
27 Cheng, S. Z. D. *Macromolecules* 1988, **21,** 2475
28 Hedmark, P. G., Werner, P.-E., Westdahl, M. and Gedde, U. W. *Polymer* 1989, **30,** 2068
29 Johnson, R. L. and Cheng, S. Z. D. *Macromolecules* 1993, **26,** 94
30 Dutta, D., Fruitwala, H., Kohli, A. and Weiss, R. A. *Polym. Eng. Sci.* 1990, **30,** 1005
31 Helminiak, T. E., Arnold, F. E. and Benner, C. L. *Polym. Prepr. Am. Chem. Soc.* 1975, **16,** 659
32 Takayanagi, M. and Ogata, T. *J. Macromol. Sci., Phys. B* 1980, **17,** 591
33 Hwang, W. F., Wiff, D. R. and Benner, C. L. *J. Macromol. Sci., Phys. B* 1983, **22,** 231
34 Wickliffe, S. M., Farris, R. J. and Malone. M. F. *J. Appl. Polym. Sci.* 1987, **34,** 931
35 Nehme, O. A., Gabriel, C. A., Farris, R. J., Thomas, E. L. and Malone, M. F. *J. Appl. Polym. Sci.* 1988. **35,** 1955
36 Nakai, A., Shiwaku, T., Hasegawa, H. and Hashimoto, T. *Macromolecules* 1986, **19,** 3008
37 Hasegawa, H., Shiwaku, T., Nakai, A. and Hashimoto, T. in 'Dynamics of Ordering Processes in Condensed Matter' (Eds S. Komura and H. Furukawa), Plenum Press, New York, 1988, p. 457
38 Kyu, T. and Zhuang, P. *Polym. Commun.* 1988, **29,** 99
39 Laivins, G. V. *Macromolecules* 1989, **22,** 3974
40 Tang, P., Reimer, J. A. and Denn, M. M. *Mcromolecules* 1993, **26,** 4269
41 Flory, P. J. *Proc. R. Soc. London, Ser. A* 1956, **234,** 73
42 Flory, P. J. *Adv. Polym. Sci.* 1984, **59,** 1
43 ten Bosch, A., Pinton, J. F., Maissa, P. and Sixou, P. *J. Phys. A* 1987, **20,** 4531

44 Lui, A. J. and Fredrickson, G. H. *Macromolecules* 1992, **25,** 5551
45 Lui, A. J. and Fredrickson, G. H. *Macromolecules* 1993, **26,** 2817
46 Nakai, A., Shiwaku, T., Wang, W., Hasegawa, H. and Hashimoto, T. *Macromolecules* in press
47 Nakai, A., Wang, W., Hashimoto, T., Blumstein, A. and Maeda, Y. *Macromolecules* 1994, **26,** 6963
48 Hashimoto, T., Suehiro, S., Shibayama, M., Saijo, K. and Kawai, H. *Polym. J.* 1981, **13,** 501
49 Suehiro, S., Saijo, K., Ohta, Y., Hashimoto, T. and Kawai, H. *Anal. Chim. Acta* 1986, **189,** 41
50 Economy, J., Storm, R. S., Matkovich, V. I., Cottis, S. G. and Nowark, B. E. *J. Polym. Sci., Polym. Chem. Edn* 1976, **14,** 2207
51 Hashimoto, T., Itakura, M. and Hasegawa, H. *J. Chem. Phys.* 1986, **85,** 6118
52 Hashimoto, T. in 'Materials Science and Technology' (Eds R. W. Cahn, P. Haasen and E. J. Kramer), Vol. 12, VCH, Weinheim, 1993, Ch. 6
53 Flory, P. J. 'Principles of Polymer Chemistry', Cornell University Press, Ithaca, NY, 1953
54 Hashimoto, T., Sasaki, K. and Kawai, H. *Macromolecules* 1984, **17,** 2812